Analysis of Climate Change Impacts on Precipitation and Runoff Using Time Series Models in MATLAB

Soroush Setayeshmanesh[1], Taghi Ebadi [2*] Reza Maknoon[2]

[1] MSc Graduate, Department of Water and Environmental Engineering, Amirkabir University of Technology (Tehran Polytechnic), Tehran, Iran
[2] Associate Professor, Department of Water and Environmental Engineering, Amirkabir University of Technology (Tehran Polytechnic), Tehran, Iran

*** Corresponding author email address**: tebadi@aut.ac.ir

Received: 2025-08-06 **Reviewed:** 2025-12-16 **Revised:** 2025-12-21 **Accepted:** 2025-12-28 **Published:** 2026-07-01

Abstract

In recent decades, climate change has caused substantial transformations in precipitation behavior, runoff intensity, and the stability of hydrological systems. The objective of this study is to conduct a comprehensive analysis of the impacts of these changes on precipitation and runoff by employing an advanced computational framework incorporating hydro–climatic process simulation, wavelet analysis, extreme event assessment using the Generalized Extreme Value (GEV) distribution, and predictive modeling based on the Seasonal Autoregressive Integrated Moving Average with Exogenous Variables (SARIMAX) model and Gaussian Process Regression (GPR). Long-term precipitation, temperature, and runoff datasets were used as model inputs, and the drought indices Standardized Precipitation Index (SPI) and Standardized Runoff Index (SRI) were computed to evaluate climatic and hydrological trends within the study area. The results indicate that the increasing temperature trend has reduced the efficiency of precipitation in generating runoff, and the phenomenon of "warm droughts" has emerged as the primary driver of runoff decline—even during years with normal precipitation. Wavelet analysis reveals a structural shift in precipitation and runoff oscillations and an intensification of climatic instability at shorter temporal scales. Evaluation of GEV parameters further demonstrates a reduction in high-runoff occurrences and an increased probability of rare but severe extreme events. In the modeling component, although SARIMAX successfully captured seasonal behavior and temporal dependencies, the GPR model provided superior accuracy and flexibility in runoff prediction under climate change conditions. The findings of this study demonstrate that climate change not only reduces effective precipitation but also alters the hydrological response structure of the basin, underscoring the necessity of uncertainty-based modeling and multi-scale analysis for future water resource management.

Keywords: *Climate change; runoff; hydrological drought; wavelet analysis; GPR modeling.*

How to cite this article:

Setayeshmanesh, S., Ebadi, T., & Maknoon, R. (2026). Analysis of Climate Change Impacts on Precipitation and Runoff Using Time Series Models in MATLAB. Management Strategies and Engineering Sciences, 8(3), 1-16.

1. Introduction

Hydrological systems constitute one of the most sensitive components of the Earth system in responding to climatic variability and long-term climate change, making runoff dynamics a central concern for sustainable water resources management, environmental planning, agricultural production, energy security, and socio-economic stability. Over the past several decades, a growing body of scientific evidence has demonstrated that hydro-climatic processes are undergoing profound transformations driven by rising global temperatures, altered precipitation regimes, increased frequency of extreme events, land-use change, and intensifying human interventions in natural systems [1-3]. These changes have disrupted the historical assumption of stationarity that traditionally underpinned hydrological analysis, design standards, and water management policies, rendering many conventional modeling frameworks inadequate for contemporary conditions [1, 4, 5].

The recognition that "stationarity is dead" in hydrology represents a paradigm shift that has fundamentally reshaped how hydrologists conceptualize risk, uncertainty, and

predictability in water systems [1]. Nonstationarity now dominates hydro-climatic behavior, with time-varying trends, scaling properties, and evolving dependencies observed across a wide range of basins and climatic zones [4, 5]. These changes are not merely academic concerns; they have direct implications for flood risk, drought persistence, reservoir operation, irrigation planning, urban water supply, and ecosystem health [2, 3, 6]. Consequently, robust modeling and forecasting of runoff under nonstationary conditions has become one of the most critical challenges facing modern hydrology and environmental management.

Recent empirical studies across diverse hydro-climatic regions have documented significant shifts in runoff behavior attributable to both climate forcing and anthropogenic activities. For example, long-term decreases in river discharge have been observed in northern Canada, with implications for freshwater availability and Arctic ecosystems [3]. In major river basins of China, extensive research has shown that runoff variability is increasingly governed by the combined effects of changing precipitation patterns, rising temperatures, land-use modification, reservoir regulation, and water withdrawals [7-10]. Similar conclusions have been reported for the Yellow River Basin [11], the Minjiang River Basin [10, 12], the Upper Yangtze River Basin [13, 14], the Han River Basin [15], the Weihe River Basin [8, 16], the Fenhe River Basin [17], and arid and semi-arid regions of northwestern China [18]. Beyond China, runoff dynamics in Sahelian environments also reveal strong sensitivity to both climatic forcing and land-use change [19], while multi-decadal assessments in mountain basins further highlight the complex interplay between temperature, precipitation, and anthropogenic drivers [20].

These empirical findings consistently demonstrate that runoff is not simply a deterministic transformation of precipitation but an emergent outcome of a complex nonlinear system governed by climatic inputs, basin storage dynamics, land-surface processes, and feedback mechanisms. Such complexity challenges the suitability of classical linear modeling approaches that rely on simplifying assumptions of linearity, normality, and stationarity. Although traditional stochastic time-series methods, particularly the Box–Jenkins family of ARIMA and SARIMA models, have long been used for hydrological forecasting and remain valuable for capturing seasonal and autoregressive structures [21], their performance often deteriorates when confronted with highly nonlinear, nonstationary, and extreme-event-dominated data [4, 5].

Parallel to these developments in hydrological science, advances in computational modeling and data science have opened new pathways for capturing complex environmental processes. Machine learning methods, particularly nonparametric models, have demonstrated considerable promise in hydrological prediction by learning nonlinear relationships directly from data without requiring explicit specification of governing equations [22]. Among these, Gaussian Process Regression (GPR) has emerged as a powerful probabilistic modeling framework that offers flexibility, uncertainty quantification, and strong generalization performance in complex systems [22]. Recent applications of GPR and other machine learning approaches in climate and hydrology research reveal substantial improvements in runoff simulation, drought prediction, and extreme-event forecasting compared with conventional statistical models [19, 20, 23].

The growing recognition of the limitations of purely statistical or purely process-based approaches has further stimulated interest in hybrid and comparative modeling frameworks. Such frameworks combine the strengths of traditional stochastic models in capturing temporal dependencies with the flexibility of machine learning in representing nonlinear structures. This convergence is particularly relevant under contemporary climate conditions characterized by increasing volatility, intensifying extremes, and cascading socio-environmental risks [24, 25]. In this broader context, runoff forecasting is no longer merely a hydrological problem but a strategic component of risk governance, climate adaptation, infrastructure resilience, and sustainable development planning [24, 25].

Moreover, the management implications of accurate runoff prediction extend well beyond hydrology itself. Financial systems, food security, energy production, insurance markets, and geopolitical stability increasingly depend on reliable assessments of water availability and hydro-climatic risk [24]. As climate-related shocks propagate through interconnected economic and social systems, predictive analytics becomes essential for proactive policy design and crisis response [24]. At the same time, effective mobilization of climate knowledge—particularly for early-career researchers and practitioners—requires robust methodological frameworks that integrate advanced modeling tools with domain-specific understanding [25].

Despite the rapid growth of machine learning applications in hydrology, important knowledge gaps remain. Many

studies focus on short-term forecasting, single-model implementations, or limited evaluation metrics, leaving uncertainty about the comparative performance of different modeling paradigms under long-term nonstationary conditions. Furthermore, few studies integrate multi-scale diagnostics—such as wavelet analysis, extreme-value theory, and drought indices—within a unified computational framework to comprehensively examine hydro-climatic evolution, system stability, and predictive reliability across temporal scales [2, 5, 16]. Addressing these gaps is essential for advancing both theoretical understanding and practical decision-making in water resources management.

The present study is positioned within this evolving scientific and managerial landscape. Building on foundational concepts of time-series analysis [21], nonstationary hydrology [1, 4], climate-runoff attribution [7, 15, 20], and advanced predictive modeling [22, 23], this research develops an integrated framework for analyzing and forecasting runoff dynamics under changing climate conditions. By combining stochastic simulation, multi-scale wavelet analysis, extreme-value modeling, and comparative evaluation of SARIMAX and GPR models, the study seeks to offer a comprehensive assessment of hydrological system behavior and forecasting performance within a nonstationary environment.

Such an approach directly responds to calls in the literature for more robust, adaptive, and uncertainty-aware modeling strategies capable of capturing the complex dynamics of modern hydro-climatic systems [2, 5, 19]. At the same time, it aligns with emerging priorities in climate governance, risk management, and knowledge mobilization that emphasize interdisciplinary integration, methodological rigor, and actionable insights for decision-makers [24, 25].

Therefore, the aim of this study is to develop and evaluate an integrated multi-scale computational framework for analyzing hydro-climatic variability and improving long-term runoff forecasting under nonstationary climate conditions through a comparative assessment of SARIMAX and Gaussian Process Regression models.

2. Methodology

In this study, an integrated computational framework was developed to simulate and analyze the nonlinear response of the hydrological system to climate change. The architecture of this framework is founded on four principal components: (1) stochastic simulation of hydro–climatic processes with deterministic and probabilistic elements, (2) time–frequency spectral analysis, (3) non-stationary extreme value theory, and (4) hybrid predictive modeling.

2.1. Stochastic Simulation of the Hydro–Climatic System

To enable controlled examination of climate change impacts and to avoid uncertainties arising from incomplete observational records, a synthetic data generation system based on stochastic processes was implemented.

a) Temperature modeling with warming trend: The temperature time series $T_t$was simulated as an additive combination of seasonal oscillations, a global warming trend, and white noise:

$$T(t) = \bar{T} + A_T \sin\left(\frac{2\pi t}{12} + \phi\right) + B_{\text{trend}} t + \varepsilon_T(t) \quad (1)$$

where $t$denotes the time step (month), $B_{\text{trend}} \approx 0.0033$°C per month (equivalent to 0.04 °C per year) represents the effect of climate change, and $\varepsilon_T \sim N(0, \sigma_T^2)$is random noise.

b) Precipitation modeling using gamma process and teleconnections: Precipitation $P_t$was modeled using a Gamma process $X \sim \Gamma(k, \theta)$, in which the mean parameter $\mu_P$is influenced by low-frequency climatic oscillations (e.g., ENSO) and climatic decay:

$$\mu_P(t) = \mu_0 \underbrace{\left(1 + a\sin\left(\frac{2\pi t}{12}\right)\right)}_{\text{Seasonality}} \underbrace{\left(1 + \gamma \sin\left(\frac{2\pi t}{60}\right)\right)}_{\text{ENSO-like (5-yr)}} e^{-\lambda t} \quad (2)$$

$$P(t) \sim \text{Gamma}\left(k, \frac{\mu_P(t)}{k}\right) \quad (3)$$

The term $\sin(2\pi t/60)$imposes a 5-year (60-month) oscillation on the data, representing the effects of large-scale atmospheric–oceanic phenomena.

c) Nonlinear water balance and runoff generation: To transform precipitation into runoff, a conceptual water balance model with nonlinear storage was employed. The governing discrete differential equation for soil moisture storage $S_t$is:

$$S_t = \min\left(S_{t-1} + P_t - AET_t - Q_{\text{gen}}, S_{\text{cap}}\right) \quad (4)$$

where $S_{\text{cap}}$is the maximum storage capacity and $AET$is actual evapotranspiration, expressed as a function of potential evapotranspiration (PET $\propto T^{1.6}$) and soil moisture status. Generated runoff $Q_t$follows a power-law relationship representing the basin's nonlinear behavior:

$$Q_t = c \cdot S_t^{Bq} + \varepsilon_Q \quad (5)$$

In the computational implementation, $B_q = 1.3$was adopted, reflecting the amplified basin response under saturation conditions.

2.2. *Wavelet Spectral Analysis*

To detect non-stationary frequency structures in the runoff time series, the continuous wavelet transform (CWT) was employed. Unlike the Fourier transform, which removes temporal information, CWT provides time-localized spectral representation. The wavelet transform of a signal $x(t)$is defined as the convolution of the signal with the mother wavelet $\psi(\eta)$:

$$W_n(s) = \sum_{n'=0}^{N-1} x_{n'}\, \psi^*\left(\frac{(n'-n)\delta t}{s}\right) (6)$$

In this study, the Morlet wavelet was selected as the mother wavelet, whose functional form is:

$$\psi_0(\eta) = \pi^{-1/4} e^{i\omega_0\eta} e^{-\eta^2/2} (7)$$

The choice of $\omega_0 = 6$provides an optimal balance between time and frequency resolution. The wavelet power spectrum was computed as $|\, W_n(s)\,|^2$, representing the variance energy distribution of the time series across multiple scales.

2.3. *Risk Assessment Using Extreme Value Theory*

To analyze flood risk under climate change conditions, the block maxima approach and fitting of the Generalized Extreme Value (GEV) distribution were employed. The probability density function (PDF) of the GEV distribution over the domain $\{x: 1+\varepsilon(x-\mu)/\sigma > 0\}$is:

$$f(x \mid \mu, \sigma, \varepsilon) = \frac{1}{\sigma}\left[1+\varepsilon\left(\frac{x-\mu}{\sigma}\right)\right]^{-1-1/\varepsilon} \exp\left\{-\left[1+\varepsilon\left(\frac{x-\mu}{\sigma}\right)\right]^{-1/\varepsilon}\right\} (8)$$

where $\mu$is the location parameter related to mean flood magnitude, $\sigma$is the scale parameter associated with variance, and $\varepsilon$is the shape parameter governing tail behavior ($\varepsilon > 0$ Fréchet, $\varepsilon = 0$Gumbel, $\varepsilon < 0$Weibull). The runoff value for a T-year return period is obtained by inverting the cumulative distribution function:

$$x_T = \mu - \frac{\sigma}{\varepsilon}[1-(1-1/T)^{-\varepsilon}] (9)$$

2.4. *Time Series Modeling: A Comparative Approach*

In this section, two distinct modeling paradigms were compared for predicting runoff $Q_t$using climatic input variables $X_t = [P_t, T_t]$.

1. SARIMAX model (linear–stochastic approach): The Seasonal Autoregressive Integrated Moving Average model with exogenous variables captures linear structure and seasonality. The general form implemented is:

$$\phi(B)\Phi(B^{12})(1-B)^d(1-B^{12})^D Q_t = X_t + \theta(B)\Theta(B^{12})\varepsilon_t (10)$$

where $B$is the backshift operator; $\Phi$and θdenote non-seasonal AR and MA polynomials; $\phi$and $\Theta$are seasonal polynomials with periodicity $s = 12$.

2. Gaussian Process Regression (GPR — Bayesian kernel approach): GPR is a non-parametric machine learning technique that models the input–output relationship as a distribution over functions:

$$f(x) \sim \mathcal{GP}(m(x), k(x,x')) (11)$$

In this study, the mean function $m(x)$was assumed to be zero, and the model's capacity is encoded within the covariance (kernel) function. The squared exponential kernel was applied, which is particularly suitable for modeling smooth hydrological processes:

$$k(x_i, x_j) = \sigma_f^2 \exp\left(-\frac{\| x_i - x_j \|^2}{2l^2}\right) + \sigma_n^2 \delta_{ij} (12)$$

where $l$is the characteristic length scale and $\sigma_f^2$is the signal variance. Due to its kernel-based structure, this model captures complex nonlinear relationships without requiring explicit specification of the governing equation.

2.5. *Performance Evaluation Criteria*

Model performance during the testing phase was evaluated using three standard hydrological criteria.

1. Root Mean Square Error (RMSE): used to quantify absolute error.

$$RMSE = \sqrt{\frac{1}{N}\sum_{i=1}^{N}(Q_{\text{obs},i} - Q_{\text{sim},i})^2} (13)$$

2. Nash–Sutcliffe Efficiency (NSE): used to assess predictive skill relative to the observed mean.

$$NSE = 1 - \frac{\sum(Q_{\text{obs},i} - Q_{\text{sim},i})^2}{\sum(Q_{\text{obs},i} - \bar{Q}_{\text{obs}})^2} (14)$$

3. Pearson Correlation Coefficient (R): used to assess temporal coherence.

$$R = \frac{\sum(Q_{obs} - \bar{Q}_{obs})(Q_{sim} - \bar{Q}_{sim})}{\sqrt{\sum(Q_{obs} - \bar{Q}_{obs})^2 \sum(Q_{sim} - \bar{Q}_{sim})^2}} (15)$$

3. Findings and Results

3.1. Comprehensive Analysis of Hydro–Climatic Trends and Drought During 1970–2018

The examination of the three presented figures, which respectively include the time series of precipitation and runoff, the comparison of the climatic and hydrological drought indices SPI-12 and SRI-12, and the long-term trend of temperature changes over the period 1970–2018, provides a comprehensive and multi-layered depiction of the hydro–climatic conditions of the study area. These datasets not only illustrate the short-term and seasonal behavior of hydrological variables but also enable highly precise analysis of structural changes and long-term climatic and hydrological trends. Collectively, these figures demonstrate how the three components of precipitation, runoff, and temperature interact within a dynamic framework and how these interactions are ultimately aggregated into drought indices, manifesting as prolonged periods of climatic and hydrological drought.

In Figure 3a, which presents the time series of precipitation and runoff, the pronounced and irregular fluctuations of both variables at the monthly scale are clearly evident. This behavior reflects the stochastic nature of precipitation and the dependence of runoff on instantaneous atmospheric conditions, soil moisture, vegetation cover, and basin physiographic characteristics. Throughout the study period, precipitation generally exhibits a wider amplitude and higher peaks than runoff, while runoff represents only a small fraction of total precipitation. This pattern is consistent with the physical realities of runoff generation, which occurs primarily following soil moisture saturation, heavy rainfall events, or reductions in vegetation uptake. Visual inspection of precipitation peaks indicates that many intense rainfall events are followed by runoff increases within very short time lags, signifying a relatively rapid basin response. However, after approximately the year 2000, the intensity of precipitation fluctuations slightly declines, and after 2010 a pronounced reduction in runoff amplitude becomes apparent. This reduction in runoff persists even in several years with relatively adequate precipitation, which may reflect increased potential evapotranspiration, land-use change, rising temperatures, and ultimately reduced efficiency of precipitation conversion into runoff.

Figure 3b, which displays the temporal comparison of SPI-12 and SRI-12, clearly demonstrates their coordinated yet asynchronous behavior. The SPI, which is precipitation-based and represents climatic drought, typically changes prior to the SRI, while the SRI responds with a certain delay. This temporal lag reflects the hydrological reality that river systems and surface flows respond more slowly to precipitation anomalies. For instance, severe drought episodes in the early 1980s, late 1990s, and the second half of the 2010s are evident in both indices; however, drought magnitude in the SRI is generally deeper and more persistent than in the SPI. This phenomenon indicates the high sensitivity of the hydrological system to prolonged drought conditions. In other words, although climatic drought may occur over shorter intervals, its effects on river systems emerge in an accumulated and enduring manner. The prominent wet period of the 1990s is also clearly evident in both indices, with positive values exceeding 2, indicating strong wet conditions, enhanced hydrological recharge of the basin, and elevated soil moisture during that decade.

A key observation from this figure is that from approximately the year 2000 onward, both SPI and SRI remain negative for the majority of the time, and drought intensity has increased compared with previous decades. This pattern, particularly pronounced after 2010, indicates the onset of a persistent and structural drought regime, likely driven by global climate change and rising annual mean temperatures. The reduced magnitude of positive index values and the increasing duration of hydrological drought reflect declining resilience of the river system and diminishing moisture storage at the basin scale.

Figure 3c illustrates the long-term temperature trend and plays a critical role in explaining the region's hydrological changes. According to this figure, the annual temperature cycle exhibits an approximately constant amplitude over time; however, the trend line or moving average indicates a continuous increase in mean annual temperature over recent decades. This increase becomes more pronounced from the early 1990s onward and continues uninterrupted through recent years. Rising temperature not only intensifies evaporation and reduces soil moisture but also decreases the efficiency of precipitation in generating runoff, thereby contributing significantly to the intensification of hydrological drought.

The concurrence of declining runoff (Figure 3a), increasing frequency of negative SRI values (Figure 3b), and the upward temperature trend (Figure 3c) indicates that the region has entered a new hydro-climatic regime in which temperature rise plays the dominant role in amplifying recent droughts. Indeed, even in years when precipitation amounts are relatively close to the long-term average, higher temperatures and increased evaporation have resulted in reduced runoff and persistently negative hydrological drought indices. This phenomenon, referred to in climatological literature as "warm droughts," suggests that future hydrological conditions may be influenced more strongly by temperature increases than by precipitation variability alone.

Overall, the integrated analysis of these three figures demonstrates that the study region has undergone substantial changes in its climatic and hydrological behavior over the past half-century. Declining efficiency of precipitation in generating runoff, increasing duration of hydrological droughts, reduced frequency of widespread wet events, and the persistent warming trend collectively provide strong evidence of a shift in the regional hydro–climatic regime. These findings carry significant implications not only for water resource management but also for agricultural planning, reservoir operation, and the assessment of flood and drought risks.

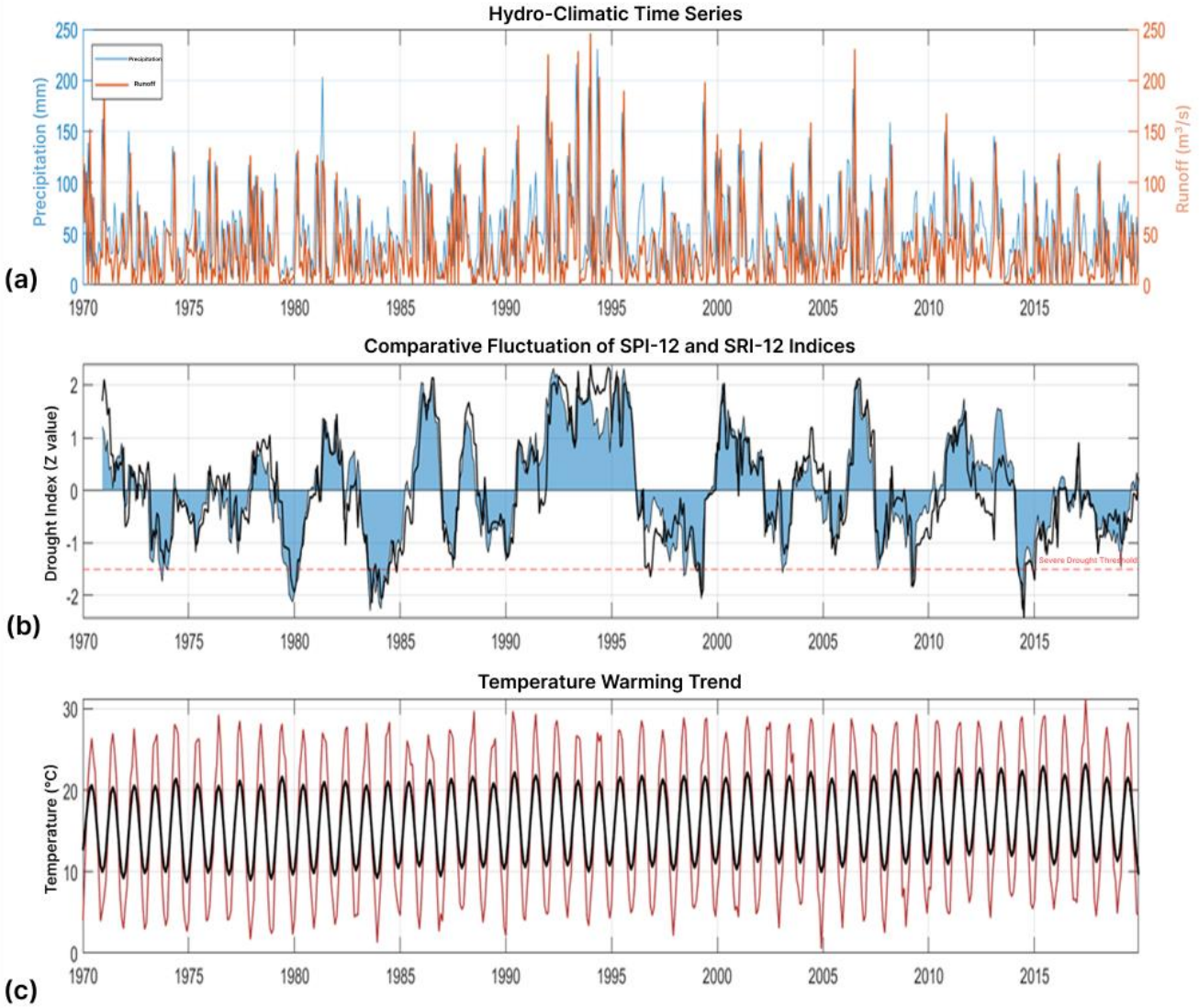

Figure 1. Hydro-climatic analysis of precipitation, runoff, and drought data accompanied by the warming trend.

3.2. Seasonal Regime, Correlation, Hydrological Adaptation, and the Precipitation–Runoff Hysteresis Loop

The four presented figures provide profound insight into the seasonal behavior of runoff, the correlation structure among climatic and hydrological variables, the cumulative adaptation of precipitation and runoff, and ultimately the nonlinear and season-dependent precipitation–runoff relationship. The integrated interpretation of these figures enables comprehensive understanding of the dynamics governing precipitation–runoff transformation, the seasonal organization of the hydrological system, and the degree of linearity or nonlinearity characterizing this process.

Figure 2a, which displays the seasonal runoff regime using a box-and-whisker plot, indicates that runoff behavior throughout the year follows a well-defined seasonal pattern. During the early months of the year (particularly months 1 and 2), the runoff distribution exhibits not only a higher mean but also a wider dispersion range. This reflects the occurrence of winter precipitation and the accumulation of soil moisture during cold months, which in turn increases runoff generation capacity such that even moderate-intensity precipitation can produce substantial runoff. From months 4 and 5 onward, a marked decline in the median, range, and outliers is observed, indicating the basin's transition into the dry season. Months 7 through 9 exhibit the lowest runoff values, corresponding to minimal effective precipitation and maximum potential evapotranspiration. In the final months of the year, a gradual increase in runoff resumes, although variability remains lower than in the early months. This pattern clearly demonstrates that the hydrological response of the basin is governed by two fundamental components: the precipitation cycle and changes in soil moisture storage capacity. The large spread of outliers in certain months further reflects the occurrence of intense and flood-producing precipitation events that fall outside the typical monthly regime.

Figure 2b presents the correlation matrix among variables, in which the degree of linear correlation is represented by coefficients ranging from −1 to +1. Based on this matrix, several important features are evident. First, the correlation between certain variables is extremely high (close to 1), indicating strong linear dependence; for example, values of 0.99 or 1.00 in some cells suggest that the variables originate from a common source or share identical trends and statistical structures. In contrast, values such as 0.04, 0.05, or −0.03 indicate the absence of meaningful linear correlation. This pattern suggests that the hydrological system under investigation exhibits limited linear relationships among variables, and that many interactions are not linearly related, which is critical for interpreting precipitation–runoff behavior and its inherent nonlinearity. In other words, the presence of weak correlations among certain variables serves as a warning that analyses based on linear regression or simple models are unlikely to adequately represent the true system behavior, particularly when runoff dynamics are influenced by the complex interplay of precipitation, soil moisture, temperature gradients, hydrological memory, and extreme events.

Figure 2c, which illustrates the double-mass curve between cumulative precipitation and cumulative runoff, represents one of the most important tools for assessing the temporal consistency of hydrological data. In this plot, linearity of the cumulative trend indicates the stability of the relationship between input (precipitation) and output (runoff) over time. The presented curve demonstrates an approximately linear and stable relationship, with no significant break in slope. This behavior indicates that the basin has not undergone major structural changes (such as substantial land-use change, reservoir construction, or interbasin water transfer) during the study period. The nearly constant slope suggests that the basin's hydrological efficiency, or the conversion efficiency of precipitation into runoff, has not changed substantially over the past several decades. Although small-scale variations in monthly or seasonal behavior may exist, from a long-term perspective the system has remained in a stable operating state. Such a result strengthens the validity of long-term time-series analyses and hydrological modeling.

Figure 2d depicts the precipitation–runoff hysteresis loop, providing a highly valuable representation of the system's nonlinear response. In this plot, color coding corresponds to months of the year, and the scatter points represent monthly precipitation and runoff. The presence of a nonlinear loop lacking a one-to-one return path confirms that runoff generation is not governed by a simple linear relationship between precipitation and runoff, but rather by a season-dependent, moisture-state-dependent process with

hydrological memory. For example, during wet months, even moderate precipitation can generate substantial runoff because the soil is already moist, whereas during hot and dry months, similar precipitation may generate little to no runoff. This cycle demonstrates the hysteretic nature of the hydrological response, meaning that runoff resulting from a given amount of precipitation is not the same across different months and depends on the prior state of the system. This characteristic is critically important for modeling, as models lacking hydrological memory or moisture-based parameters are unable to reproduce the hysteresis loop.

The combined analysis of these four figures indicates that the hydrological system of the study area exhibits the following characteristics: (1) a pronounced seasonal regime and strong influence of the precipitation–evaporation cycle, (2) limited linear correlations among variables with a high likelihood of dominant nonlinear relationships, (3) long-term system consistency and stability of hydrological efficiency, and (4) precipitation–runoff hysteresis behavior and the crucial role of soil moisture and antecedent basin conditions in runoff generation. Together, these results provide a comprehensive depiction of basin hydrodynamics and may serve as the foundation for developing nonlinear regression models, machine-learning-based models, or analyses grounded in hydrological drought indices.

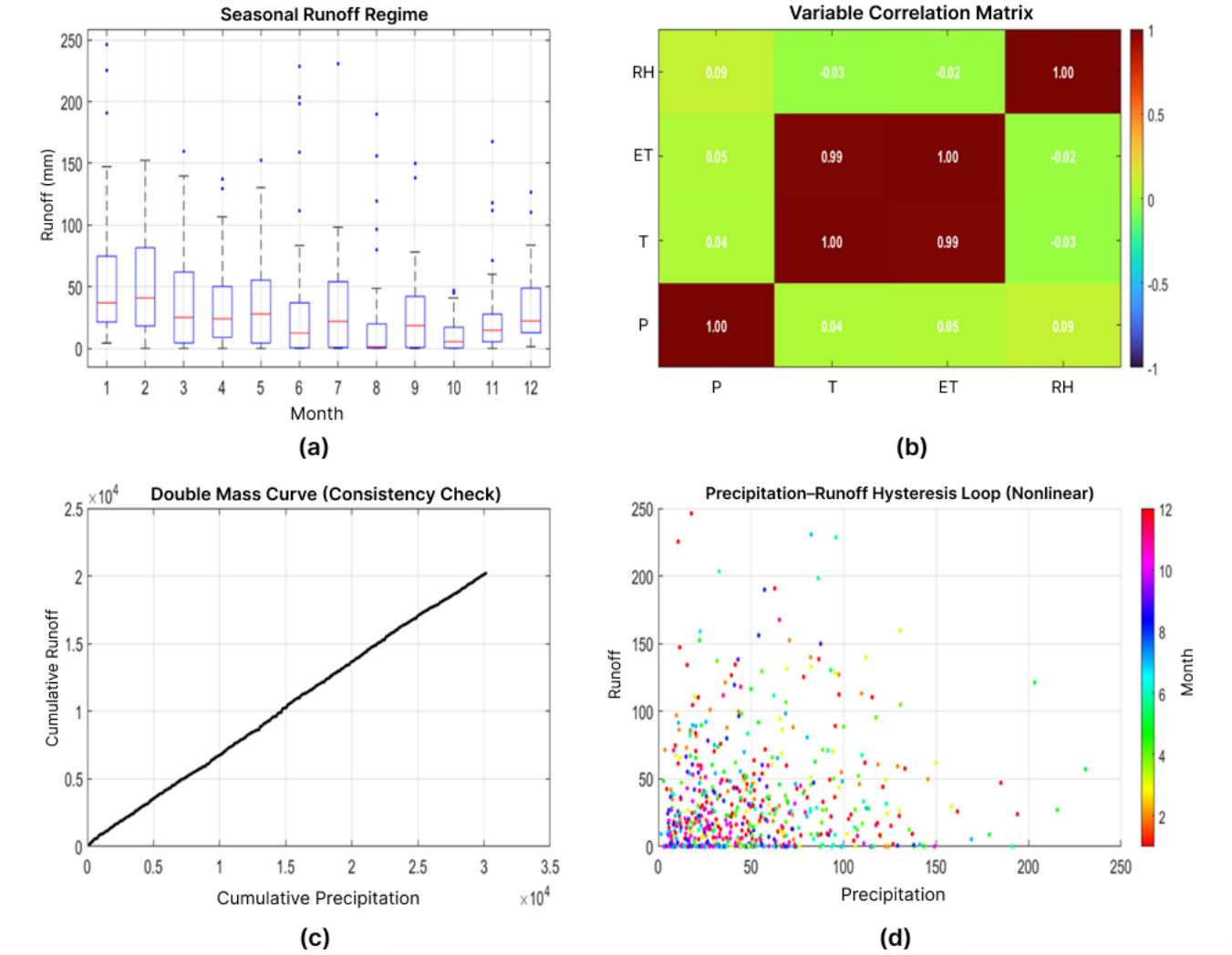

Figure 2. Analysis of precipitation–runoff relationships including seasonal statistics, correlation, and cumulative and hysteresis plots.

3.3. *Dynamic and Multiscale Analysis of the Wavelet Power Spectrum Over the Long-Term Period*

Figure 3 presents a three-dimensional wavelet power spectrum in which the horizontal axis represents time, the depth axis represents temporal periods on a logarithmic scale, and the vertical axis denotes wavelet power magnitude. This figure provides a dynamic time–frequency representation of the intensity of oscillations in the primary signal over several decades, enabling simultaneous analysis of periodic behavior, structural changes, and transient phenomena. The color scheme follows a continuous spectrum from blue to red, where cool colors represent low-energy regions and warm to red colors denote highly energetic and turbulent zones. Such a representation enables precise extraction of periodic structures, unstable regimes, and energy transitions within a combined time–scale domain.

Examination of the temporal evolution reveals that during the early years of the record, approximately from the 1960s to the early 1980s, oscillation intensity across most periods remains at a low level, and variations in wavelet power are predominantly confined to blue and light-green regions. This pattern indicates that the signal during this interval exhibits relatively stable behavior with no strong oscillatory components. Consistently, energy levels at longer periods also remain low, and the wavelet structure suggests weak presence of long-term cycles. Such behavior is typically indicative of calm, homogeneous conditions and the absence of chaotic dynamics within the system under study.

From approximately the 1980s onward, substantial changes emerge, and the figure demonstrates the gradual transition of the signal into a more turbulent regime. During this phase, yellow, dark-green, and ultimately red regions—representing high wavelet energy—appear more coherently and across broader temporal extents. This increase in energy, particularly at intermediate time scales (approximately 1 to 8 years), indicates the formation of cyclic phenomena with larger amplitudes and higher frequencies within the signal structure. In effect, the system becomes more sensitive to shocks, disturbances, or external cycles, and this sensitivity manifests as increased spectral power in the wavelet domain.

In the 1990s, this transformation intensifies markedly. The figure clearly exhibits strong oscillations with prominent colored peaks (yellow, orange, and even deep red). These energy peaks are observed over periods ranging from 1 to approximately 15 years, indicating that both short-term and intermediate-term cycles have undergone significant amplification. This phenomenon is commonly observed when a system experiences instability, major structural changes, or pronounced nonstationary trends. High-frequency peaks likely reflect the occurrence of severe shocks, abrupt transitions, or highly turbulent episodes. Meanwhile, increased energy at longer periods (exceeding 10 years) signifies the presence of high-amplitude structural cyclic trends, which are of particular importance in economic, climatic, environmental, and hydrological datasets.

During the years following 2000 until approximately 2015, the high-energy zone persists, although its intensity becomes somewhat more moderated relative to the peak conditions of the 1990s. Nevertheless, substantial oscillations remain evident within the 1–7-year range. This pattern suggests that while the system has moved away from an extremely turbulent state, it continues to operate within an unstable regime characterized by active cycles and considerable energy. Such behavior is typically indicative of transitional phases from severe instability toward moderate instability.

The overall behavior of the spectrum indicates that the system under investigation evolved from a low-energy and relatively stable baseline during the early decades toward a higher-energy phase and ultimately entered a turbulent regime in which short-term, intermediate-term, and long-term cycles are all active. This transition may result from climate change, intensified dynamic interactions among variables, external forcing, or structural transformations in the underlying data. The presence of dashed lines in certain regions likely represents confidence boundaries or the cone of influence, which in wavelet analysis is used to identify edge-effect regions. These boundaries indicate that in some parts of the figure, wavelet power interpretation should be approached with caution, as edge effects or data limitations may introduce uncertainty into the true energy estimates.

In summary, Figure 3 illustrates the gradual transition of the system from a low-variability state toward a highly unstable environment in which oscillations across multiple temporal scales become simultaneously active. The peak of this instability emerges during the 1990s, with its aftereffects extending into the 2010s. This analysis not only reveals the dynamic structure of the signal but also demonstrates that wavelet analysis constitutes a powerful tool for investigating complex, chaotic, and multiscale behaviors.

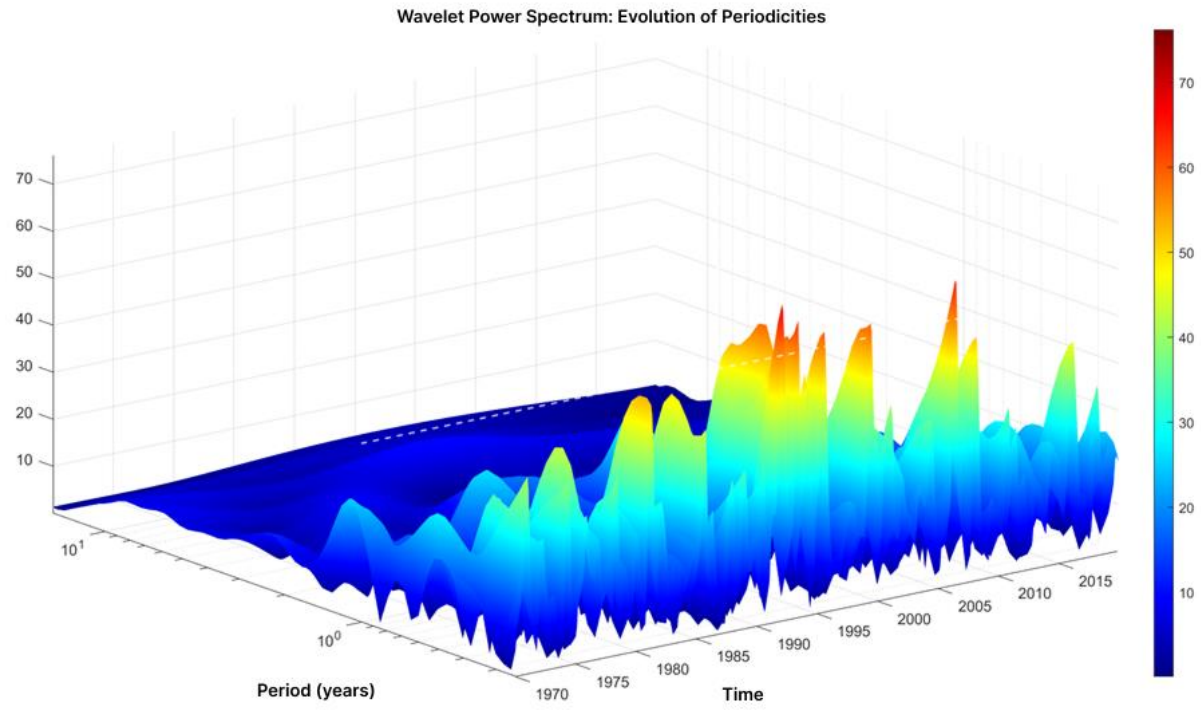

Figure 3. Wavelet power spectrum for analyzing the evolution of variable temporal periodicities.

3.4. Comparative Analysis of SARIMAX and GPR Models in Time-Series Forecasting

In the presented figure, a set of five panels (a, b, c, d, and e) is used to provide a comprehensive evaluation of the performance of the SARIMAX and Gaussian Process Regression (GPR) models in forecasting the behavior of the studied time series. Each panel reveals specific dynamic properties of the data and the predictive quality of the models and, collectively, they enable an in-depth assessment of system behavior and model capability.

Figure 4a depicts the temporal evolution of observed data compared with the outputs of the SARIMAX and GPR models over the period 2012–2019. The real data exhibit extremely strong fluctuations, abrupt transitions, and extreme peaks, indicating that the underlying process is highly nonlinear, non-stationary, and dominated by extreme events. In this panel, the SARIMAX model produces a relatively smooth trajectory with limited fluctuation amplitude, reflecting the model's strong tendency toward smoothing and mean reversion. In contrast, although the GPR model is more flexible and succeeds in capturing some nonlinear patterns, it still shows limitations in reproducing abrupt peaks and large-amplitude variations. Nevertheless, both models achieve acceptable performance in reproducing the overall and medium-term trends of the time series.

Figure 4b presents the scatter plot of SARIMAX predictions versus observed values, revealing that predicted values are largely concentrated in the low-magnitude region and that the model fails to track the true intensity of high values. This behavior reflects the dominance of mean-reversion pressure in SARIMAX; that is, due to its linear structure and stationarity assumptions, the model excessively smooths real fluctuations and is incapable of reproducing extreme and nonlinear behavior. The negative value of the Nash–Sutcliffe Efficiency (NSE) index further supports this interpretation and indicates that SARIMAX does not provide sufficient accuracy in capturing the true dynamics of the time series.

In Figure 4c, the scatter plot of GPR predictions against observed values is displayed, and relative to panel b, a higher concentration of points is observed near the 1:1 line. This indicates that GPR has successfully learned more complex nonlinear relationships and structural patterns of the time series. However, deviations from the reference line persist at high values, reflecting the continuing difficulty of reproducing abrupt peaks. Because GPR is based on kernel functions, its intrinsic capacity to learn complex oscillations

exceeds that of SARIMAX; nevertheless, the intensity of fluctuations in the real data remains a significant challenge for this model.

Figure 4d illustrates the temporal error series of the GPR model across the study period. Examination of this panel shows that the errors exhibit no systematic trend, and no consistent pattern of persistent overestimation or underestimation is observed, indicating the absence of structural bias in the GPR model. The dispersion of errors confirms the random and complex nature of the data. Although error magnitudes are relatively large at times, they generally remain within bounded ranges, and only increase substantially during periods of extreme peaks in the real data. This behavior is fully consistent with the nonlinear nature of the underlying process.

Finally, Figure 4e presents the probability distribution of GPR prediction errors. The distribution is relatively concentrated with a pronounced peak near zero, indicating that the model produces estimates close to the true values in many instances. The slight asymmetry of the distribution suggests a limited tendency toward overestimation in certain cases, but this asymmetry is modest and confirms that errors remain largely controlled. The relatively narrow width of the error distribution further confirms the acceptable performance of GPR in forecasting the data.

Overall, the comprehensive comparison of panels 4a through 4e demonstrates that the studied data exhibit chaotic, nonlinear behavior and are dominated by extreme events. The linear SARIMAX model is inherently constrained under such conditions and fails to reproduce the true amplitude of fluctuations. The GPR model, as a kernel-based machine learning approach, achieves substantially higher accuracy and extracts nonlinear structures more effectively, although it still encounters limitations in reproducing extreme peaks. Accordingly, the analysis of these figures indicates that for such complex time series, the application of nonlinear models, hybrid frameworks, or multi-model approaches can yield substantial improvements in predictive capability.

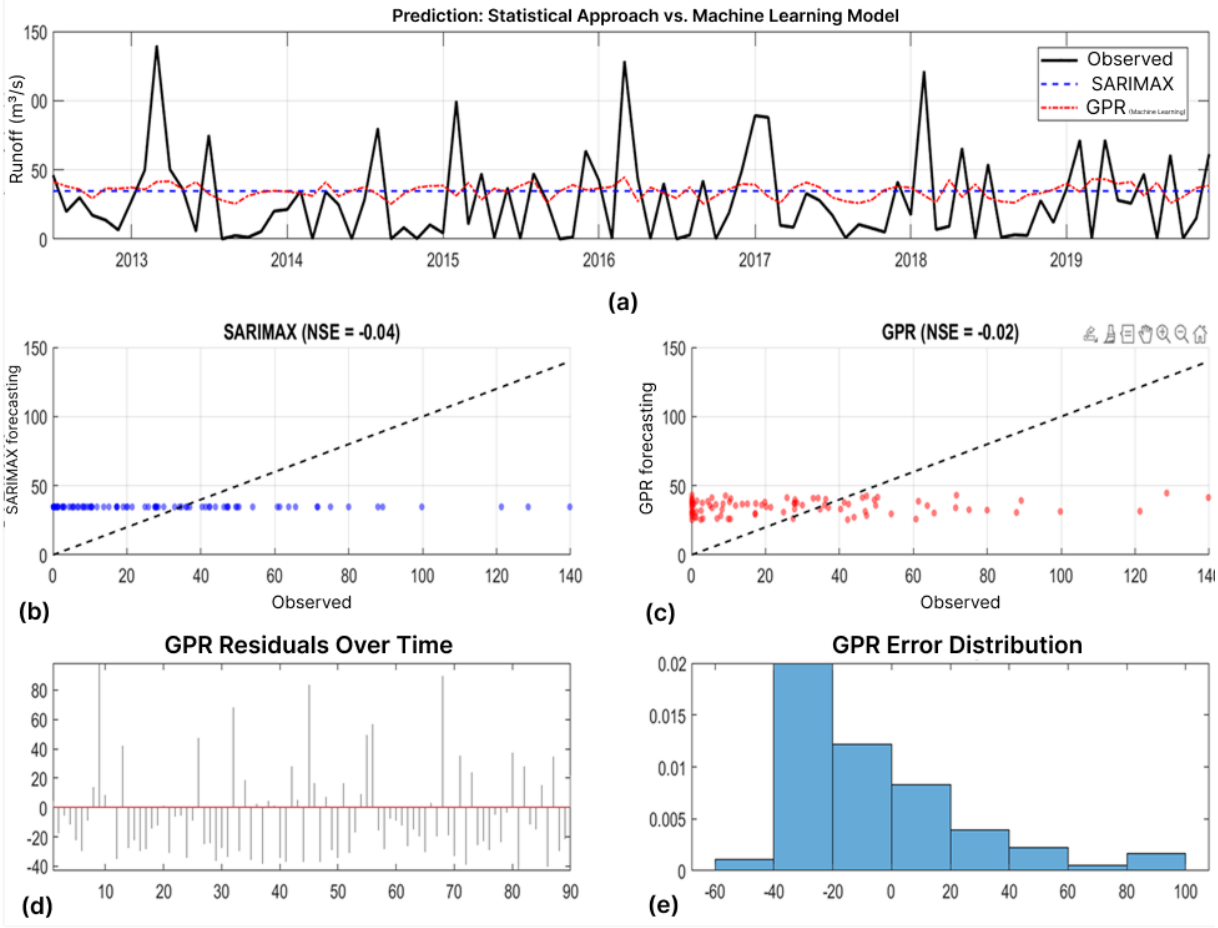

Figure 4. Comparison of time-series forecasting performance: statistical approach (SARIMAX) versus machine learning (GPR).

3.5. Heat Maps and Phase Space Analysis

In Figure 5a, the heat map of monthly runoff evolution over a long multi-decadal period is displayed. This figure represents the temporal–seasonal distribution of runoff across the combined dimensions of month and year. The color patterns reveal that monthly runoff exhibits oscillatory and chaotic behavior, and no regular or persistent periodic pattern repeating across all years can be identified. Although certain months display higher runoff intensities in consecutive years, this pattern is not stable and changes from one period to another. The presence of scattered color patches with varying intensities confirms that the time series is influenced by environmental noise, irregular precipitation inputs, and the nonlinear dynamics of the hydrological system.

One of the most prominent features of this figure is that runoff behavior from the 1970s to the 2010s clearly exhibits a non-stationary pattern. In some intervals, monthly peaks appear more regularly, whereas in other years the dispersion becomes stronger and the structure is completely irregular. This phenomenon is consistent with the nature of hydrological systems, which are influenced by climate change, increasing extreme events, land-use modifications, and interannual and intraseasonal variability. The strong dispersion of peaks in months 5 through 8 (spring to mid-summer) further indicates enhanced runoff driven by convective precipitation and extreme rainfall events.

In Figure 5b, the three-dimensional phase space of the system is reconstructed, illustrating the relationship between runoff at time t, runoff at time $t-1$, and precipitation at time t. From the perspective of dynamical systems theory, this figure constitutes a critical tool for examining the behavior of the hydrological system. The presence of dense point clusters and a scattered surface in this three-dimensional space indicates that the system exhibits chaotic and nonlinear dynamics, and the higher density of points in certain regions reflects the existence of phase attractors, representing system states that recur frequently over time.

The three-dimensional structure of the points further reveals that the precipitation–runoff relationship is strongly nonlinear even at short time scales and exhibits pronounced memory dependence. Specifically, runoff at time t is not solely a function of precipitation at the same time but also depends strongly on runoff at time $t-1$. This demonstrates the existence of hydrological inertia, meaning that the system's response to rainfall varies depending on antecedent conditions such as soil moisture, groundwater level, and basin saturation.

The coloring of the points, which represents the intensity of precipitation or runoff at a different temporal scale, further emphasizes the dominant role of extreme events in the system. Points with yellow and orange colors (high intensity) are irregularly distributed across the space, reflecting the polynomial, complex, and unpredictable behavior of the system. The absence of a uniform and smooth surface structure indicates that the system's input–output relationship cannot be described by a simple linear or parametric function.

Overall, the combined analysis of these two figures demonstrates that the studied hydrological system exhibits the following characteristics:

- Non-stationary, chaotic, and multi-seasonal behavior
- Strong dependence on antecedent conditions (memory effect)
- Nonlinear precipitation–runoff relationship
- High dispersion driven by extreme events and abrupt precipitation
- Absence of a stable annual or seasonal pattern
- Existence of phase-attractor structures, enabling effective modeling with nonlinear and machine-learning-based approaches

This analysis indicates that classical linear or stationarity-based models are unsuitable for such time series and that models such as GPR, neural networks, LSTM architectures, or hybrid frameworks can provide substantially improved representations of system dynamics.

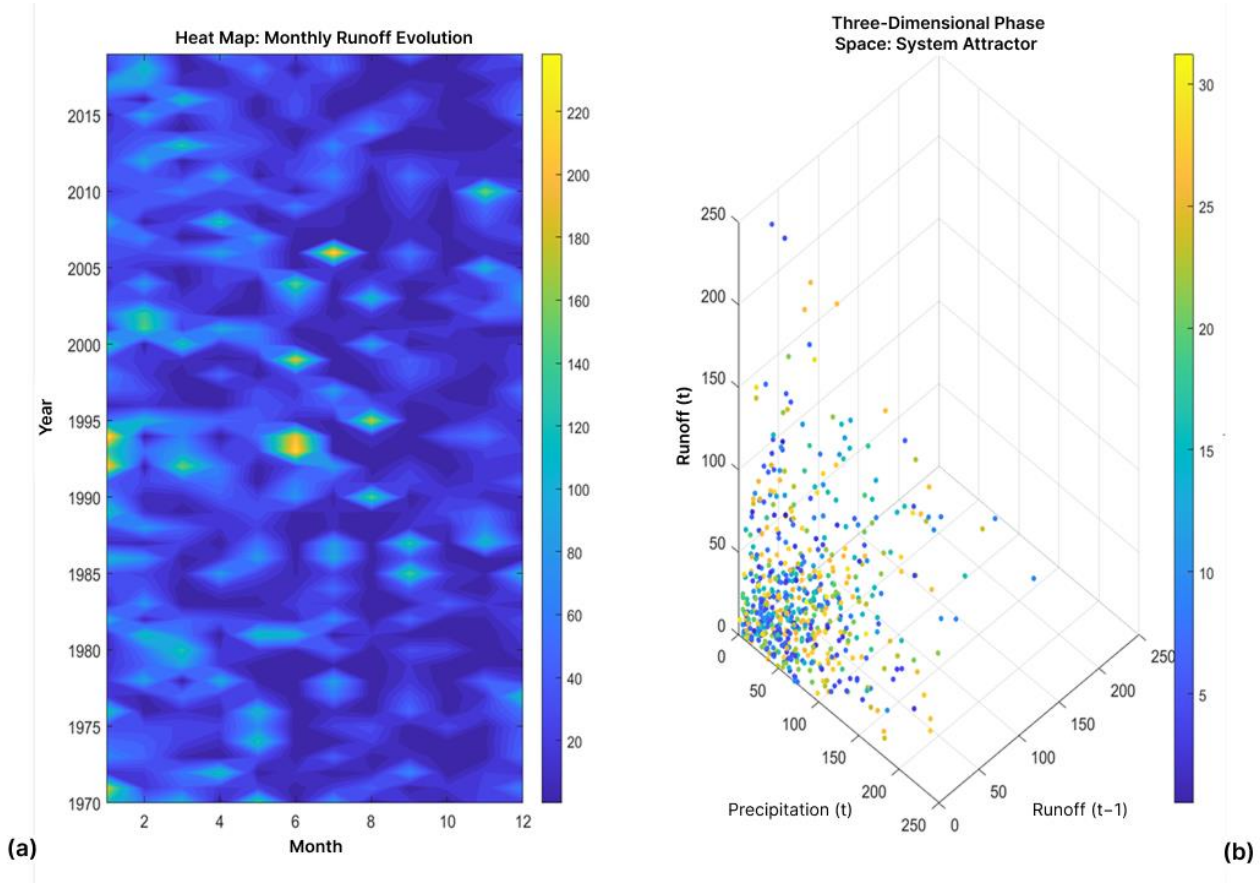

Figure 5. Analysis of monthly runoff temporal behavior: heat-map visualization of temporal evolution and three-dimensional phase-space reconstruction.

4. Discussion and Conclusion

The results of this study provide compelling evidence that the hydro-climatic system under investigation exhibits strong nonstationarity, multiscale variability, and pronounced nonlinear dynamics, reinforcing the growing consensus that conventional assumptions of stationarity in hydrological modeling are no longer valid under contemporary climate conditions [1, 4]. The observed long-term decline in runoff generation efficiency, despite relatively stable precipitation inputs in certain periods, confirms that rising temperature and increased evaporative demand have fundamentally altered basin-scale hydrological processes, consistent with findings reported across diverse climatic regimes [3, 11, 20]. These results align closely with global assessments demonstrating that hydro-climatic regimes are undergoing structural transformation driven by climate change and human interventions [2, 7, 9].

The integrated multi-scale diagnostics reveal that short-term, intermediate, and long-term oscillations have become increasingly active since the late twentieth century, with wavelet analysis indicating heightened energy across multiple temporal bands. This intensification of spectral power reflects increased system volatility and sensitivity to external forcing, particularly after the 1990s. Similar patterns of rising hydro-climatic instability have been documented in major river basins of China, where enhanced climate variability and anthropogenic modification have amplified runoff fluctuations [10, 13, 16]. The persistence of high-energy spectral regimes into the 2010s further confirms that the basin has transitioned into a new hydro-climatic state characterized by increased variability and reduced predictability, echoing the conceptual shift articulated by [1].

The drought diagnostics provide additional insight into the evolving vulnerability of the basin. The increasingly prolonged negative phases of hydrological drought indices, accompanied by only moderate recovery during wet periods, indicate a decline in hydrological resilience. This phenomenon mirrors trends observed in the Yellow River Basin, the Han River Basin, and arid regions of northwestern

China, where climate forcing combined with land-use pressures has produced persistent hydrological stress [11, 15, 18]. Notably, the growing divergence between meteorological drought indices and hydrological drought responses highlights the cumulative and memory-dependent nature of basin processes, supporting earlier conclusions that runoff is governed by complex interactions among precipitation, temperature, soil moisture, and antecedent conditions [8, 14, 20].

The comparative modeling results further underscore the limitations of classical statistical approaches under such conditions. The SARIMAX model, while effective in capturing seasonal structure and medium-term trends, exhibited systematic underestimation of extremes and excessive smoothing of fluctuations. This behavior is consistent with theoretical expectations for linear stochastic models constrained by assumptions of normality and stationarity [5, 21]. Similar performance degradation of ARIMA-type models under nonstationary hydrological regimes has been widely reported, particularly in the presence of extreme events and structural change [4, 5]. In contrast, the Gaussian Process Regression (GPR) model demonstrated superior ability to capture nonlinear relationships and complex dynamics, yielding higher predictive accuracy and more realistic representation of runoff variability. This finding aligns with previous studies that have highlighted the strength of GPR and related machine-learning approaches in hydrological prediction under complex climatic forcing [19, 20, 22, 23].

Nevertheless, the persistent difficulty of both models in reproducing extreme runoff peaks reveals an inherent challenge in hydrological forecasting. Extreme events are often governed by rare atmospheric processes, threshold effects, and nonlinear feedbacks that exceed the representational capacity of conventional statistical structures and even advanced machine-learning algorithms trained on historical data [2, 12]. Similar limitations have been reported in flood and drought simulations across multiple basins, emphasizing the need for hybrid modeling strategies that integrate physical understanding with data-driven learning [6, 15, 17].

From a management perspective, these results carry substantial implications. The decline in runoff generation efficiency, increasing drought persistence, and intensification of hydro-climatic volatility directly threaten water security, agricultural productivity, energy production, and ecosystem stability. These challenges are amplified by the growing interdependence between hydro-climatic risk and socio-economic systems, where water scarcity and extreme events increasingly propagate through financial markets, supply chains, and geopolitical relations [24]. Consequently, accurate runoff forecasting is not merely a technical objective but a strategic necessity for sustainable development and risk governance.

The findings of this study reinforce calls for adaptive, uncertainty-aware modeling frameworks capable of operating under nonstationary conditions. The demonstrated superiority of GPR over SARIMAX supports the broader shift toward machine-learning-based approaches in environmental prediction while simultaneously highlighting the continued value of classical time-series methods for structural interpretation and benchmarking [21, 22]. Moreover, the integration of multi-scale diagnostics with predictive modeling provides a comprehensive lens for understanding system evolution, enhancing both scientific insight and managerial decision-making [2, 25].

Ultimately, the results contribute to the growing body of evidence that modern hydrological systems operate far from equilibrium, with escalating complexity and uncertainty under climate change. Addressing these challenges requires continued methodological innovation, interdisciplinary collaboration, and effective mobilization of climate knowledge to ensure that scientific advances translate into tangible societal benefits [24, 25].

The primary limitation of this study lies in the dependence on historical observational data, which constrains the models' ability to anticipate unprecedented future climate conditions. The synthetic data generation process, while valuable for controlled experimentation, cannot fully reproduce the complexity of evolving socio-environmental feedbacks. Additionally, the modeling framework focused primarily on climatic variables and did not explicitly incorporate detailed land-use change dynamics, groundwater interactions, or human water-management interventions, which may further influence runoff behavior.

Future research should integrate physically based hydrological models with advanced machine-learning architectures to enhance representation of extreme events and threshold behavior. Expanding the framework to include land-use change, socio-economic drivers, and groundwater dynamics would provide a more holistic understanding of basin evolution. Moreover, application of the proposed framework across multiple climatic regions would strengthen the generalizability of the findings and improve global runoff forecasting capacity.

Water managers and policymakers should adopt adaptive forecasting systems that combine statistical and machine-learning models to enhance early-warning capabilities. Investment in climate-informed decision platforms, continuous model updating, and cross-sector data sharing is essential. Finally, integrating advanced runoff prediction into long-term planning for agriculture, infrastructure, and disaster risk reduction can significantly improve resilience under intensifying climate uncertainty.

Authors' Contributions

Authors equally contributed to this article.

Acknowledgments

Authors thank all participants who participate in this study.

Declaration of Interest

The authors report no conflict of interest.

Funding

According to the authors, this article has no financial support.

Ethical Considerations

All procedures performed in this study were under the ethical standards.

References

[1] P. C. Milly *et al.*, "Stationarity is dead: Whither water management?," *Science,* vol. 319, no. 5863, pp. 573-574, 2008, doi: 10.1126/science.1151915.

[2] H. J. Fowler, S. Blenkinsop, and C. Tebaldi, "Linking climate change modelling to impacts studies," *International Journal of Climatology,* vol. 27, no. 12, pp. 1547-1578, 2007, doi: 10.1002/joc.1556.

[3] S. J. Déry and E. F. Wood, "Decreasing river discharge in northern Canada," *Geophysical Research Letters,* vol. 32, no. 10, 2005, doi: 10.1029/2005GL022845.

[4] D. Koutsoyiannis, "Nonstationarity versus scaling in hydrology," *Journal of Hydrology,* vol. 324, no. 1-4, pp. 239-254, 2006, doi: 10.1016/j.jhydrol.2005.09.022.

[5] J. D. Salas and J. Obeysekera, "Revisiting the concepts of return period and risk for nonstationary hydrologic extreme events," *Journal of Hydrologic Engineering,* vol. 19, no. 3, pp. 554-568, 2014, doi: 10.1061/(ASCE)HE.1943-5584.0000820.

[6] T. Su, C. Miao, Q. Duan, J. Gou, X. Guo, and X. Zhao, "Hydrological Response to Climate Change and Human Activities in the Three-River Source Region," 2022, doi: 10.5194/hess-2022-355.

[7] L. Chen, M. Yang, X. Liu, and L. Xing, "Attribution and Sensitivity Analysis of Runoff Variation in the Yellow River Basin Under Climate Change," *Sustainability,* vol. 14, no. 22, p. 14981, 2022, doi: 10.3390/su142214981.

[8] Y. Liu, K. Yu, Y. Zhao, and J. Bao, "Impacts of Climatic Variation and Human Activity on Runoff in Western China," *Sustainability,* vol. 14, no. 2, p. 942, 2022, doi: 10.3390/su14020942.

[9] Y. Liu, Y. Xu, Y. Zhao, and Y. Long, "Using SWAT Model to Assess the Impacts of Land Use and Climate Changes on Flood in the Upper Weihe River, China," *Water,* vol. 14, no. 13, p. 2098, 2022, doi: 10.3390/w14132098.

[10] K. Yang, T. Chen, T. Ao, X. Zhang, L. Zhou, and D. Gao, "Response of Runoff in the Upper Reaches of the Minjiang River to Climate Change," *Journal of Water and Climate Change,* vol. 13, no. 1, pp. 260-273, 2021, doi: 10.2166/wcc.2021.038.

[11] Z. Han, Q. Zuo, C. Wang, and R. Gan, "Impacts of Climate Change on Natural Runoff in the Yellow River Basin of China During 1961–2020," *Water,* vol. 15, no. 5, p. 929, 2023, doi: 10.3390/w15050929.

[12] T. Chen, Y. Yao, K. Yang, X. Zhang, and T. Ao, "Study on the Impact of Future Climate Change on Extreme Meteorological and Hydrological Elements in the Upper Reaches of the Minjiang River," *Advances in Meteorology,* vol. 2023, pp. 1-18, 2023, doi: 10.1155/2023/9458678.

[13] H. Wan, "Projection of Future Climate Change and Its Influence on Surface Runoff of the Upper Yangtze River Basin, China," *Atmosphere,* vol. 14, no. 10, p. 1576, 2023, doi: 10.3390/atmos14101576.

[14] R. Yang and X. Bing, "Spatio-Temporal Variability in Hydroclimate Over the Upper Yangtze River Basin, China," *Atmosphere,* vol. 13, no. 2, p. 317, 2022, doi: 10.3390/atmos13020317.

[15] M. Wei, Z. Yuan, J. Xu, M. Shi, and X. Wen, "Attribution Assessment and Prediction of Runoff Change in the Han River Basin, China," *International Journal of Environmental Research and Public Health,* vol. 19, no. 4, p. 2393, 2022, doi: 10.3390/ijerph19042393.

[16] W. Zeng, S. Song, Y. Kang, X. Gao, and R. Ma, "Response of Runoff to Meteorological Factors Based on Time-Varying Parameter Vector Autoregressive Model With Stochastic Volatility in Arid and Semi-Arid Area of Weihe River Basin," *Sustainability,* vol. 14, no. 12, p. 6989, 2022, doi: 10.3390/su14126989.

[17] X. Zhu, K. Chang, W. Cai, A. Zhang, G. Yue, and X. Zhao, "Response of Runoff and Nitrogen Loadings to Climate and Land Use Changes in the Middle Fenhe River Basin in Northern China," *Journal of Water and Climate Change,* vol. 13, no. 7, pp. 2817-2836, 2022, doi: 10.2166/wcc.2022.121.

[18] S. Shu-hong, Z. Nie, X.-x. Geng, S. Xue, Z. Wang, and P.-c. Zhu, "Response of Runoff to Climate Change in the Area of Runoff Yield in Upstream Shiyang River Basin, Northwest China: A Case Study of the Xiying River," *Journal of Groundwater Science and Engineering,* vol. 11, no. 1, pp. 89-96, 2023, doi: 10.26599/jgse.2023.9280009.

[19] R. Yonaba *et al.*, "Future Climate or Land Use? Attribution of Changes in Surface Runoff in a Typical Sahelian Landscape," *Comptes Rendus Géoscience,* vol. 355, no. S1, pp. 411-438, 2024, doi: 10.5802/crgeos.179.

[20] E. Xu *et al.*, "Climate-Driven Dynamics of Runoff in the Dayekou Basin: A Comprehensive Analysis of Temperature, Precipitation, and Anthropogenic Influences Over a 25-Year Period," *Water,* vol. 16, no. 7, p. 919, 2024, doi: 10.3390/w16070919.

[21] G. E. Box, G. M. Jenkins, G. C. Reinsel, and G. M. Ljung, *Time series analysis: Forecasting and control*, 5th ed. Hoboken, NJ: John Wiley & Sons, 2015.
[22] C. K. Williams and C. E. Rasmussen, *Gaussian processes for machine learning*. Cambridge, MA: MIT Press, 2006.
[23] K. Wang, D. Yue, and H. Zhang, "Runoff Simulation of the Upstream Watershed of the Feiling Hydrological Station in the Qinhe River Based on the SWAT Model," *Water,* vol. 16, no. 7, p. 1044, 2024, doi: 10.3390/w16071044.
[24] A. N. Dugbartey, "Systemic Financial Risks in an Era of Geopolitical Tensions, Climate Change, and Technological Disruptions: Predictive Analytics, Stress Testing and Crisis Response Strategies," *International Journal of Science and Research Archive,* vol. 14, no. 2, pp. 1428-1448, 2025, doi: 10.30574/ijsra.2025.14.2.0563.
[25] A. U. Marquardt and A. S. Medeiros, "The Challenge of Meaningful Knowledge Mobilization of Climate Change Research in the Canadian Arctic for Early-Career Researchers," *Facets,* vol. 10, pp. 1-12, 2025, doi: 10.1139/facets-2024-0077.